ORGANOMETALLICS

Article

pubs.acs.org/Organometallics

Monosubstituted Borane Ruthenium Complexes $RuH_2(\eta^2{:}\eta^2\text{-}H_2BR)(PR'_3)_2$: A General Approach to the Geminal Bis(σ-B−H) Coordination Mode

Yann Gloaguen,[†,‡] Gaëtan Bénac-Lestrille,[†,‡] Laure Vendier,[†,‡] Ulrike Helmstedt,[§,⊥] Eric Clot,*[,§] Gilles Alcaraz,*[,†,‡] and Sylviane Sabo-Etienne*[,†,‡]

[†]LCC (Laboratoire de Chimie de Coordination), CNRS, BP44099, 205 Route de Narbonne, F-31077 Toulouse Cedex 4, France

[‡]Université de Toulouse, UPS, INPT, F-31077 Toulouse, France

[§]Institut Charles Gerhardt, CNRS 5253, Université Montpellier 2, cc 1501, Place Eugène Bataillon, 34095 Montpellier, France

Supporting Information

ABSTRACT: A series of borane bis(σ-B−H) ruthenium complexes $RuH_2(\eta^2{:}\eta^2\text{-}H_2BR)(PR'_3)_2$ (R = alkyl, aryl; R′ = Cy, Cyp, ^{i}Pr) has been prepared by using two synthetic strategies. The first one is based on a simple substitution reaction by adding the corresponding monosubstituted H_2BR borane to the bis(dihydrogen) ruthenium complex $RuH_2(\eta^2\text{-}H_2)_2(PCy_3)_2$. The second one, more general, results from the reaction of the chloro complex $RuHCl(H_2)(PR'_3)_2$ (R′ = Cy, Cyp, ^{i}Pr) with the corresponding lithium monosubstituted borohydrides RBH_3Li (R = Mes, ^{t}Bu, Me, C_4H_3S, Ph). All the complexes have been characterized by multinuclear NMR, IR, and X-ray diffraction studies. DFT calculations have been used to better define the bonding mode of the borane ligand to the metal center as well as to establish the thermodynamic cycle that delineates the coordination process. The ^{t}Bu species displays a dynamic behavior evidencing an equilibrium between a borohydride and a σ-borane formulation. The thienyl case illustrates the competition between sulfur coordination and a bis(σ-B−H) coordination mode.

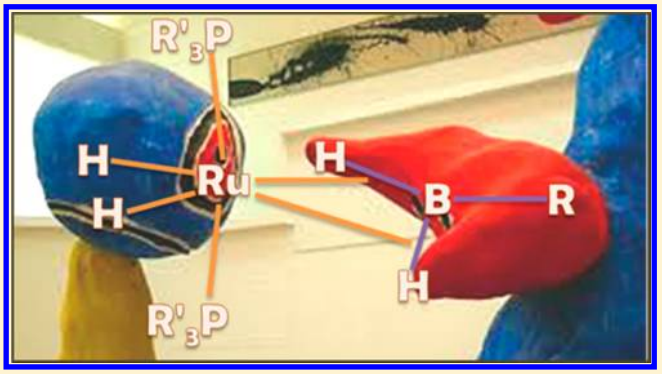

INTRODUCTION

We recently disclosed the bis(σ-B−H) coordination mode between a monosubstituted borane (RBH_2) and a metal center from the addition of RBH_2 to a polyhydride metal precursor. The prototypical example of this new family of complexes, $RuH_2(\eta^2{:}\eta^2\text{-}H_2BMes)(PCy_3)_2$ (**1**), resulted from the coordination of one molecule of mesitylborane to the $[RuH_2(PCy_3)_2]$ ruthenium fragment through two geminal σ-B−H bonds. The borane bonding mode involves a four-center−four-electron interaction between the ruthenium center and the "H−B(sp^2)−H" moiety of mesitylborane.[1,2] Related complexes incorporating monosubstituted boranes (RBH_2) to a hydrido metal fragment are rare and mostly limited to the weak Lewis acid aminoboranes $R_{2-n}H_nN{-}BH_2$ (n = 0−2).[3−10] Their recent development derives from metal-catalyzed dehydrogenation of the corresponding amine-boranes $R_{3-n}NH_n{-}BH_3$ (n = 1−3). Understanding and controlling the dehydrogenation process of this class of compounds is still attracting a lot of interest, as they are considered as potential hydrogen source and storage materials.[3−12]

The σ-borane coordination mode is reminiscent of the classical model of Chatt, Dewar, and Duncanson for the olefin−metal interaction with an additional contribution due to the presence of an empty p orbital on boron.[13,14] In contrast to aminoboranes, for which the empty p orbital on boron is strongly stabilized by donation from the adjacent nitrogen lone pair, alkyl or arylboranes present a marked Lewis acid character. When using conventional disubstituted boranes (HBpin, HBcat, 9-BBN), earlier studies on the resulting bis(tricyclohexylphosphine) ruthenium complexes showed that the Lewis acid properties of the borane influenced its coordination mode. Three limit structures could be observed featuring a σ-ligand, a σ-ligand with additional interaction between the boron and a neighboring terminal hydride, or a borohydride unit.[15−18] Promoting the bis(σ-B−H) coordination mode from a ligated borohydride motif remains an isolated case, nicely illustrated by Stradiotto et al. via chlorine abstraction from $[Cp^*Ru(P^iPr_3)(\kappa^2\text{-}H_2BMesCl)]$.[19]

To evaluate the scope of the bis(σ-B−H) coordination mode and better define its properties, we selected various Lewis acidic monosubstituted alkyl and arylboranes and built a series of ruthenium complexes stabilized by different phosphines. In this article, we focus on spectroscopic and structural data in order to evaluate the level of the B−H activation with the help of theoretical calculations.

Received: June 25, 2013

   dx.doi.org/10.1021/om400610k | *Organometallics* XXXX, XXX, XXX−XXX

Scheme 1. Synthesis of Geminal Bis(σ-B−H) Borane Ruthenium Complexes

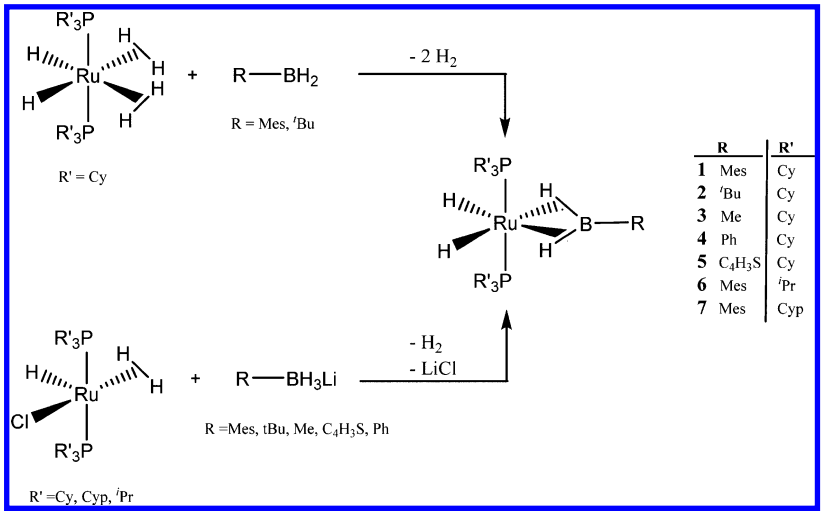

Scheme 2. Redistribution of Monosubstituted Boranes

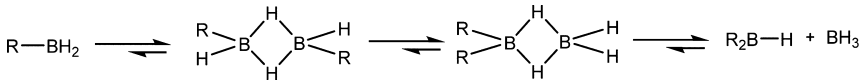

RESULTS AND DISCUSSION

Synthesis of Borane Bis(σ-B−H) Ruthenium Complexes $RuH_2(\eta^2{:}\eta^2\text{-}H_2BR)(PR'_3)_2$ (R = alkyl, aryl; R′ = Cy, Cyp, ^{i}Pr). In the previously reported communications, we showed that treatment of $RuH_2(\eta^2\text{-}H_2)_2(PCy_3)_2$ with monosubstituted boranes RBH_2 (R = Mes, ^{t}Bu) was the most direct and straightforward method to give the corresponding complexes $RuH_2(\eta^2{:}\eta^2\text{-}H_2BR)(PCy_3)_2$ (R = Mes (**1**), ^{t}Bu (**2**)) in high yield by simple dihydrogen exchange reaction (Scheme 1).[1,20] However, this method suffers from some limitations, intrinsic to the stability of the precursors. With less sterically demanding phosphine ligands than tricyclohexylphosphine, the ruthenium dihydride bis(dihydrogen) precursors are more difficult to handle and less stable, particularly with respect to loss of H_2.[21−23] In addition, this synthetic strategy is restricted to the use of stable monosubstituted boranes, which exist in a very limited number due to their propensity to rearrange into borane and the corresponding disubstituted borane (Scheme 2).[24,25] In order to develop a viable synthetic approach to a variety of borane bis(σ-B−H) ruthenium complexes, we explored a pathway that combines hydride transfer, loss of dihydrogen, and salt elimination in a one-pot procedure[1] from stable and storable monosubstituted lithium borohydrides and chlorohydrido(dihydrogen) ruthenium complexes (Scheme 1).

$RuHCl(H_2)(PR'_3)_2$ (R′ = Cy, Cyp, ^{i}Pr) precursors were obtained in high yield on a multigram scale from $[Ru(COD)Cl_2]_n$ according to known procedures.[26] The lithium monosubstituted borohydrides RBH_3Li (R = Mes, ^{t}Bu, Me, C_4H_3S, Ph) were also obtained in fairly good quantity by treatment of their respective boronate precursors with $LiAlH_4$.[27] The target borane bis(σ-B−H) ruthenium complexes could be obtained pure and in high yield from the stoichiometric reaction of the aforementioned precursors emphasizing the viability of this synthetic approach. Complexes **3**−**7** were fully characterized by IR and NMR spectroscopy and by X-ray diffraction crystallography (*vide infra*). The borane coordination mode was also studied by conducting a full optimization at the DFT/B3PW91 level of the PCy_3 series (**1**−**5**, see Computational Details).

Spectroscopic Characterization of the Bis(σ-B−H) Ruthenium Complexes. σ-B−H complexes are often considered as intermediates in the microreversible process of oxidative addition of the B−H bond to a metal center. In the case of a ruthenium polyhydride fragment, the presence of both terminal hydrides and Ru−H−B bridging hydrogens makes these systems highly dynamic, often preventing an unambiguous formulation only on the basis of multinuclear NMR data.[28] The situation is even more complicated in the case of the coordination of bidentate boranes containing an L−BH (L = P, S) moiety.[29,30]

The solid-state infrared spectra for complexes **1**−**7** present a similar profile in the frequency region between 1780 and 1985 cm^{-1}. The first set of broad shape and medium to weak intensity absorption bands is assigned to the terminal hydrides Ru−H with vibration frequencies observed between 1900 and 1985 cm^{-1}. The second set of weaker intensity but also of broad shape is located at lower frequencies, in the 1780 to 1864 cm^{-1} region, and corresponds to the Ru−H−B vibrations (Table 1). The frequency range observed for the Ru−H and Ru−H−B vibrations in **1**−**7** clearly differs from the B−H stretching frequencies of the corresponding lithium borohydrides ($2100 < \nu_{BH} < 2250$ cm^{-1})[27] or monosubstituted borane dimers[31] that are observed at even higher frequencies ($2500 < \nu_{BH} < 2605$ cm^{-1}) when reported (Table 1). For the five complexes **1**−**5** optimized at the B3PW91 level, the calculated IR spectra featured four bands in the range 1750−2000 cm^{-1} (Table 1). The two higher frequencies correspond essentially to Ru−H modes, while the two remaining modes of weaker intensities correspond to Ru−H−B vibrations. Comparison between the experimental and calculated values reveals that the agreement is overall satisfactory.

Homogeneous NMR data were collected, and a similar trend for the hydride, boron, and phosphorus chemical shifts was observed for all the complexes (Table 2). The $^{11}B\{^1H\}$ NMR spectra of **1**−**7** show a broad signal between δ +54 and +69.

dx.doi.org/10.1021/om400610k | *Organometallics* XXXX, XXX, XXX−XXX

Table 1. Experimental and Computed (*in italics*) IR Vibrational Frequencies (cm^{-1}) for the Modes Involving the Hydrides and the Hydrogen Atoms Bonded to Boron[a]

	$RuH_2(H_2BR)(PR'_3)_2$				$(RBH_2)_2$	RBH_3Li
	R	R′	ν_{Ru-H}	ν_{Ru-H-B}	ν_{BH}	ν_{BH}
1	Mes	Cy	1948 (m br)	1829 (w br)	2501 (m br)	2236 and 2203 (s br)
			1936 (m br)			
			1965 (140)	*1893 (23)*	*2501 (150)*	
			1925 (80)	*1824 (24)*		
2	^{t}Bu	Cy	1948 (w br)	1780 (w br)	2605[31]	2155 (s br)
			1964 (98)	*1863 (24)*	*2524 (150)*	
			1938 (76)	*1777 (41)*		
3	Me	Cy	1889 (w br)	1785 (w br)	n.r.	2221, 2185, and 2142 (s br)
			1964 (102)	*1851 (25)*		
			1924 (84)	*1772 (24)*		
4	Ph	Cy	1980 (m s)	1858 (w br)	2512[31]	2299, 2249 (m, br), and 2108 (s, br)
			1917 (w br)	1805 (w br)		
			1962 (126)	*1876 (26)*	*2523 (150)*	
			1924 (85)	*1793 (16)*		
5	C_4H_3S	Cy	1985 (m br)	1864 (w br)	n.r.	2258, 2225, and 2200 (m br)
			1915 (w br)	1801 (w br)		
			1974 (125)	*1911 (7)*		
			1934 (103)	*1815 (5)*		
6	Mes	^{i}Pr	1930 (m br)	1847 (w br)		
7	Mes	Cyp	1970 (w br)	1833 (m br)		
			1897 (m s)			

[a]The computed values in italics have been scaled by 0.9572,[32] and the intensities are given in parentheses.

Table 2. Selected NMR Chemical Shifts (δ) for Complexes 1−7

	^1H			
complex	RuH_2	RuH_2B	$^{31}P\{^1H\}$	$^{11}B\{^1H\}$
1	−11.26 (t)	−6.10 (br)	83.78	58
2	−10.99 (t)	−6.48 (br)	84.03	69
3	−11.06 (t)	−6.22 (br)	81.48	66
4	−11.11 (td)	−5.60 (br)	81.60	61
5	−11.95 (td)	−5.80 (br)	80.27	54
6	−11.24 (td)	−6.04 (br)	96.84	57
7	−11.08 (t)	−6.18 (br)	88.77	57

In the case of complexes incorporating PCy_3 at ruthenium (**1**−**5**), the small variation in the chemical shift is illustrative of the electronic effects induced by the substituent at boron as observed in the case of free boranes.[33] With alkyl substituents only exerting a positive inductive effect at boron, one can observe more deshielded signals (δ 69 (**2**), 66 (**3**)). The introduction of aryl substituents that supply electron density to the boron by a positive resonance results in more shielded signals (δ 61 (**4**), 58 (**1**), 54 (**5**)) compared to the alkyl analogues. The $^{31}P\{^1H\}$ NMR spectra display a sharp singlet found in a narrow range for the PCy_3 complexes (δ +80 to δ +84). All the ^1H NMR spectra exhibit at 298 K in the hydride region a characteristic set of two signals in a 1:1 ratio: a shielded triplet around δ −11 that collapses upon phosphorus decoupling ($^2J_{PH} \approx 25$ Hz) corresponding to the terminal hydrides, and a broad signal close to δ −6 that sharpens upon boron decoupling and thus assigned to the hydrogen atoms attached to boron (Supporting Information, Figure S1). No direct $^1J_{BH}$ coupling constant could be measured. In the case of coordinated mesitylborane in complexes **6** and **7**, the nature of the phosphines has no significant influence on the hydride and boron chemical shifts with respect to the prototypical complex **1**. In the case of $RuH_2(\eta^2{:}\eta^2\text{-}H_2BMes)(P^iPr_3)_2$ (**6**), better resolution of the signals in the hydride zone of the ^1H NMR spectrum was observed, and the resonance at δ −11.24 appeared as a triplet of doublets. Upon selective proton decoupling at δ −6.04, the signal collapsed into a sharp triplet, indicating the presence of a small J_{HH} coupling constant (3 Hz) between the terminal hydrides and the hydrogen attached to boron (Supporting Information, Figure S2).

The case of the thienylborane complex **5** is particularly interesting, as it highlights the stabilization brought by the bis σ-B−H ligation. The presence of a potential coordinating sulfur atom in the thienyl ring could influence the linkage of the thienylborane at the metal, as reported in the case of the reaction of $MeSCH_2BH_2MeLi$ with $RuHCl(H_2)(PCy_3)_2$, leading to the formation of the hydroborate complex $[RuH\{(\mu\text{-}H)_2(BMeCH_2SMe)\}(PCy_3)_2]$ (**8**).[29] Variable-temperature ^1H NMR spectra of **5** showed no change on cooling to 180 K, excluding the presence in solution of any borohydride linkage potentially leading to **5′** (similar to **8**) or to an agostic species (**5″**) resulting from sulfur coordination and one B−H bond of the BH_2 moiety (Scheme 3).

DFT calculations were carried out to probe the relative energy of **5′** and **5″** with respect to **5**. Figure 1 displays the geometry of various optimized isomers, together with their relative Gibbs energy. All of them are higher in energy with respect to **5**. A structure featuring both σ(B−H) coordination and S coordination (**5″** in Scheme 3) could not be located on the potential energy surface. Instead, two isomers featuring either S coordination (**5a**, Figure 1) or σ(B−H) coordination (**5b**, Figure 1) were optimized. Their geometry is typical of 16-electron Ru-dihydride complexes with one hydride ligand trans to a vacant site and the other one trans to the weakest ligand, here S or σ(B−H). The energies of **5a** and **5b** relative to **5** are similar (ΔG = 72.5 kJ·mol^{-1}, **5a**; ΔG = 72.1 kJ·mol^{-1}, **5b**) and

dx.doi.org/10.1021/om400610k | *Organometallics* XXXX, XXX, XXX−XXX

Scheme 3. Possible Coordination Modes of Thienylborane at Ruthenium

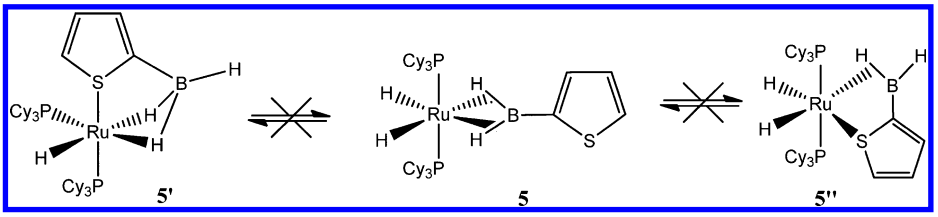

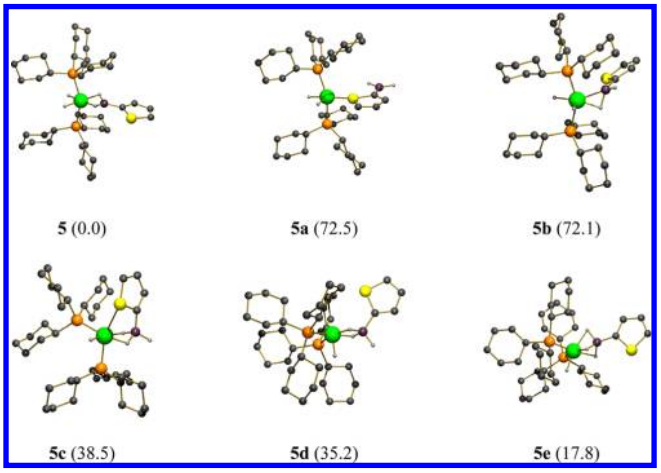

Figure 1. Optimized geometry and relative Gibbs energy (kJ·mol^{-1}) of the optimized isomers for $H_2BC_4H_3S$ interacting with $[Ru(H)_2(PCy_3)_2]$. Most H atoms are omitted for clarity.

much too high for either complex to be observed. The optimized structure **5c** (Figure 1) is similar to the bonding pattern shown in **5′** (Scheme 3). **5c** features a borohydride coordinated to $[RuH(PCy_3)_2]^+$ through two B−H bonds and a Ru···S interaction (Ru···S = 2.806 Å). Another possibility would have been to put the two phosphine ligands in the equatorial plane, thus leading to structure **5d** with no Ru···S interaction trans to the hydride (Ru···S = 3.873 Å). The loss of Ru···S coordination has been compensated by the optimal position of the hydride trans to a vacant site, and **5d** has a Gibbs energy similar to that of **5c** (ΔG = 35.2 kJ·mol^{-1} and 38.5 kJ·mol^{-1}, respectively). Finally, **5e**, the closest isomer to **5** (ΔG = 17.8 kJ·mol^{-1}, Figure 1) displays a borohydride interacting with Ru through its three hydrogen atoms. The B−H bond (1.303 Å) in pseudotrans position with respect to Ru−H is the least activated. The two other B−H bonds (1.343 and 1.397 Å) are activated to different extents as a result of different Ru−P bond lengths.

Deeper investigation of the properties of the *tert*-butylborane complex **2** evidenced a dynamic behavior undetected during our previous study.[20] The $^{31}P\{^1H\}$ NMR spectrum recorded at 298 K of a deuterated toluene solution prepared by solubilizing crystals of **2** exhibits a persistent set of two singlets at δ +84.03 and +77.3 in approximately a 3:1 ratio indicating the presence of two phosphorus-containing species. This ratio appeared temperature dependent (Supporting Information, Figure S3) and illustrates the existence of an equilibrium characterized by an equilibrium constant K_{eq} of 3 at 298 K, leading to a $\Delta_rG°$ value close to zero (*vide infra*). In the hydride zone of the ^1H NMR spectrum at 298 K, only the well-resolved signals in a 1:1 ratio corresponding to **2** could be clearly seen. At lower temperatures, three new resonances attributed to the borohydride complex **2′** were observed (Scheme 4). At 233 K, the new signals are a broad signal at δ −4.41, a broad

Scheme 4. Equilibrium between the Bis(σ-B−H) and the Borohydride Ruthenium Complexes 2 and 2′

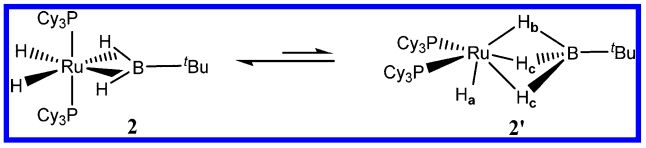

doublet at δ −9.25, and a sharp triplet at δ −14.13 in a 1:2:1 integration ratio, respectively (Supporting Information, Figure S4). The two broad signals that sharpened upon boron decoupling and collapsed into singlets upon ^{31}P decoupling are assigned to the bridging hydrogens H_b (δ −4.41) and H_c (δ −9.25) in **2′**. The sharp triplet that collapsed into a singlet in the $^1H\{^{11}B\}$-$\{^{31}P$ δ77$\}$ NMR spectrum is attributed to H_a (δ −14.13) (Supporting Information, Figure S5). No coupling constant between ^{11}B and ^1H could be measured, but a HMQC $^{11}B\{^1H\}/^1H$ experiment recorded at 273 K clearly showed the correlation of the hydrides of **2** and **2′** with a boron atom resonating at δ +69 (**2**) and at δ +39 (**2′**) (Supporting Information, Figures S6 and S7). The observation at this temperature of a high-field-shifted signal ($\Delta\delta$ +30) is in agreement with a borohydride formulation for **2′**. A 2D ^1H-EXSY experiment carried out at different temperatures illustrates the dynamic behavior of this system. At 273 K, the presence in the spectrum of cross-peaks between all the hydrides of **2** and **2′** indicates the two species are interconverting. At 233 K, only the hydrides (H_a, H_b, and H_c) in **2′** are exchanging, and no other cross-peak in the hydride zone is observed (Supporting Information, Figure S8). This corroborates the borohydride character of **2′** since borohydride complexes are known to undergo hydrogen exchange processes with low activation barriers.[34,35]

The geometries of **2** and **2′** were optimized, and the resulting structures are shown in Figure 2. The calculated geometry for **2** is in excellent agreement with experiment (*vide infra* Table 3). The borohydride ligand in **2′** presents two similar hydrogen

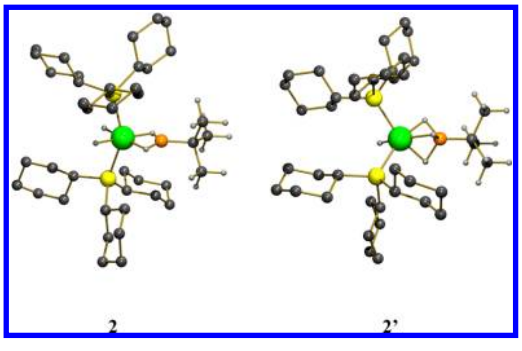

Figure 2. Optimized geometry for **2** and **2′**. Most H atoms are omitted for clarity.

dx.doi.org/10.1021/om400610k | *Organometallics* XXXX, XXX, XXX−XXX

Table 3. Comparison between Selected Distances (Å) and Angles (deg) for the X-ray and DFT/B3PW91 Calculated Structures[a] of Complexes 1−5 and Selected Distances (Å) and Angles (deg) for the X-ray Structures of Complexes 6 and 7

	1[1] exp/*calc*	2[20] exp/*calc*	3 exp/*calc*	4 exp/*calc*	5 exp/*calc*	6 exp	7[b] exp
Ru−B	1.938(4)	1.934(2)	1.947(6)	1.923(8)	1.960(6)	1.959(2)	1.961(4)/1.953(5)
	1.957	*1.945*	*1.936*	*1.942*	*1.946*		
Ru−P1	2.3186(9)	2.3159(4)	2.2866(12)	2.3057(18)	2.3297(12)	2.3052(3)	2.3151(9)/2.3047(10)
	2.362	*2.356*	*2.326*	*2.338*	*2.337*		
Ru−P2	2.2952(9)	2.3059(4)	2.3448(12)	2.3183(18)	2.3364(12)	2.3052(3)	2.3079(9)/2.3070(9)
	2.338	*2.346*	*2.370*	*2.363*	*2.366*		
B−C1	1.543(5)	1.582(3)	1.537(8)	1.541(10)	1.518(8)	1.548(3)	1.559(5)/1.549(6)
	1.554	*1.590*	*1.569*	*1.551*	*1.537*		
Ru···Hy1	1.73(3)	1.69(2)	1.79(4)	1.76(6)	1.56(4)	1.72(2)	1.64(5)/1.84(5)
	1.778	*1.777*	*1.809*	*1.806*	*1.826*		
Ru···Hy2	1.77(3)	1.73(2)	1.81(4)	1.80(6)	1.90(5)	1.68(2)	1.71(4)/1.67(4)
	1.788	*1.793*	*1.785*	*1.784*	*1.795*		
Ru−Hy3	1.61(3)	1.53(3)	1.34(4)	1.42(6)	1.55(4)	1.54(3)	1.51(4)/1.54(4)
	1.608	*1.607*	*1.606*	*1.605*	*1.611*		
Ru−Hy4	1.59(3)	1.55(2)	1.62(4)	1.71(6)	1.39(4)	1.53(2)	1.5894[c]/1.7259[c]
	1.614	*1.612*	*1.615*	*1.614*	*1.600*		
B−Hy1	1.24(3)	1.25(2)	1.18(4)	1.38(6)	1.09(4)	1.26(2)	1.27(4)/1.32(5)
	1.324	*1.334*	*1.322*	*1.318*	*1.307*		
B−Hy2	1.29(3)	1.23(2)	1.33(4)	1.32(6)	1.36(5)	1.28(2)	1.19(4)/1.27(4)
	1.315	*1.328*	*1.333*	*1.328*	*1.321*		
P1−Ru−P2	150.87(3)	151.691(16)	149.23(4)	154.18(7)	152.93(5)	158.335(18)	152.61(3)/150.68(4)
	152.1	*149.51*	*153.73*	*153.8*	*153.79*		
Ru−B−C1	177.1(3)	173.29(17)	168.1(4)	173.6(6)	175.2(4)	179.36(15)	177.8(3)/178.5(3)
	177.4	*178.63*	*173.40*	*176.7*	*174.84*		
∑B	359.72	359.35	356.22	358.84	359.23	360.00	359.95/359.25

[a]The computed values for the selected distances and angles of **1**−**5** are in italics. [b]**7** displays two independent molecules in the asymmetric unit. [c]Hy4 could not be properly refined.

atoms H_c (Ru−H_c = 1.768 and 1.770 Å; B−H_c = 1.366 and 1.384 Å) each in pseudotrans position with respect to the phosphorus atoms. The third one, H_b, is pseudotrans to the hydride H_a and, consequently, is associated with a longer Ru···H_b distance of 1.916 Å and to a shorter B−H_b bond of 1.312 Å.

Experimentally, the van't Hoff plot of the equilibrium constant obtained by integration from both the ^{1}H and the ^{31}P NMR spectra recorded over the temperature range 298−233 K provided a set of thermodynamic parameters $\Delta H°$ and $\Delta S°$ ($\Delta H°_{(1H)}$ = −12.4 ± 2.5 kJ·mol^{-1}, $\Delta H°_{(31P)}$ = −8.0 ± 0.8 kJ·mol^{-1}, $\Delta S°_{(1H)}$ = −54 ± 10 J·mol^{-1}.K^{-1}, $\Delta S°_{(31P)}$ = −36 ± 3 J·mol^{-1}·K^{-1} with 95% confidence limits) (Supporting Information, Figure S9). Broadness of the signals in the ^{1}H NMR spectra might explain the differences obtained from the two techniques. The rather high negative entropy value might result from the change in degrees of freedom from **2** to **2′**. DFT calculations were first performed without any dispersion corrections. The enthalpy value sets **2′** at 0.5 kJ·mol^{-1} above **2**, but the computed Gibbs energy difference is in good agreement with the experiment ($\Delta G°_{(calc)}$ = −5.6 kJ·mol^{-1} vs $\Delta G°_{(exp)}$ = −2.7 to −3.7 kJ·mol^{-1}). When D3 dispersion corrections are included, the enthalpy of **2′** drops 2.2 kJ·mol^{-1} below that of **2**, in better agreement with the experiment. However, the Gibbs free energy difference is now $\Delta_r G°$ = +5.8 kJ·mol^{-1}. Overall, with or without dispersion corrections, the two complexes **2** and **2′** are very close in energy, and the difference, with **2** being ca. 5 kJ mol^{-1} more or less stable than **2′**, falls within the error range of the calculations.

Structural Characterization of the Bis(σ-B−H) Ruthenium Complexes. The X-ray crystal structures of compounds **3**−**7** were recorded at 110 K. Views of complexes **3**, **5**, and **6** are given in Figure 4 (see also Figure S10 for **4** and Figure S11 for **7** in the Supporting Information). Selected geometrical parameters are provided in Table 3 as well as those previously published for **1** and **2**.[1,20] The atom numbering follows the one given in Figure 3. It can be seen that homogeneous data have been obtained for this series of bis(σ-B−H) ruthenium complexes. The Ru atom is in a pseudo-octahedral environment with the phosphines (P1 and P2) in axial positions. Four coplanar hydrogen atoms (Hy1, Hy2, Hy3, and Hy4) occupy the equatorial coordination sites of the ruthenium. The interaction between the ruthenium and the boron atom is illustrated by a Ru−B distance that is shorter than the sum of the covalent radii (2.09 Å), being between 1.923(8) and 1.961(4) Å (Table 3). A similar distance (1.9212(2) Å) was observed in the cationic ruthenium complex [Cp*Ru(η^2:η^2-H_2BMes)(P^iPr_3)]$^+$$BAr^F{}_4^-$.[36] In **1**−**7**, the P1−Ru−P2 angle lies between 149.23° and 158.33°, indicating that the phosphines are bending away from the borane ligand. In this series, the P1−Ru−P2 angles are indeed smaller than in the $PCyp_3$ bis(dihydrogen) complex $RuH_2(\eta^2\text{-}H_2)_2(PCyp_3)_2$ (168.64(2)° by X-ray, 168.9(1)° by neutron),[22] which remains the only

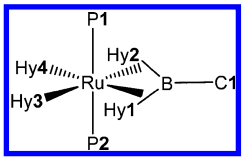

Figure 3. Atom numbering in complexes **1**−**7**.

dx.doi.org/10.1021/om400610k | *Organometallics* XXXX, XXX, XXX−XXX

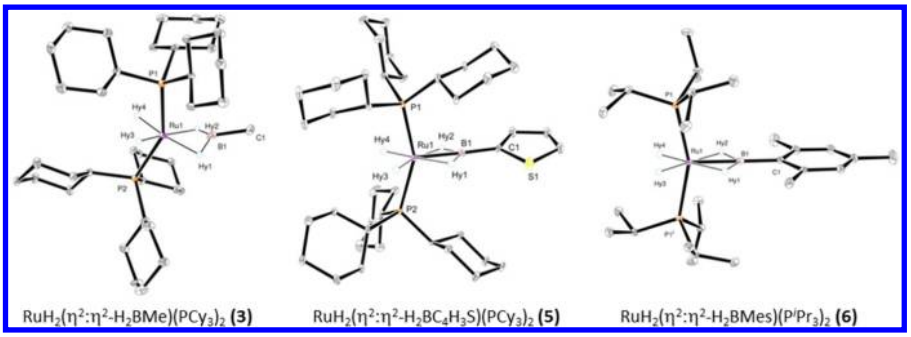

Figure 4. X-ray structures of complexes **3**, **5**, and **6**. Ellipsoids are set at the 30% level. The hydrogen atoms not associated with the metal are omitted for clarity.

Table 4. Computed X−H Bond Distances (X = H, B; Å) for the Free and Coordinated Ligands in the (Dihydrogen) and Borane Complexes and Reaction Energy and Energy Components (kJ·mol^{-1}) Associated with the Substitution of Two H_2 Molecules by H_2BR[a]

		$Ru(H)_2(H_2BR)(PCy_3)_2$				
	$Ru(H)_2(H_2)_2(PCy_3)_2$	**1**	**2**	**3**	**4**	**5**
X−H (free)	0.743	1.197	1.200	1.200	1.200	1.197
X−H (coord)	0.887	1.323	1.333	1.334	1.328	1.307
	0.878	1.316	1.328	1.322	1.318	1.321
ΔE_{smd}	0	−7.1	−12.1	−29.3	−21.3	−14.6
ΔE_{dist}(Ru)	22.2	38.9	40.5	31.8	32.2	32.2
ΔE_{dist}(L)	57.3	36.8	38.9	43.9	34.7	35.1
ΔE_{int}(Ru−L)	−223.6	−227.4	−236.2	−249.1	−232.8	−226.1
ΔE_{bond}(Ru−L)	−144.6	−151.7	−156.8	−173.5	−165.5	−158.8

[a]See Scheme 5 for definition of energy terms.

bis(dihydrogen) complex characterized by unambiguous structural data.[37,21] In the borane series, the larger value is observed with the less hindered phosphine P^iPr_3 in **6** (P1−Ru−P2 = 158.332(18)°). The quality of the data enabled the secure location of the hydrogen atoms around the ruthenium from difference Fourier electron density maps. They were freely refined except for Hy4 in complex **7**, which displays two independent molecules in the asymmetric unit. In all the complexes, sp^2-hybridization of the boron atom is ascertained by its trigonal planar environment, as evidenced by the sum of the H−B−C1 and H−B−H angles ($\sum$B, Table 3). The deviation from planarity ($360 - \sum B$) is around 1° except for **3**, which is notably more distorted (ca. 4°), with the Ru−B−C1 angle diverging from linearity by 11.9(4)°.

Computational Studies of the Bis-σ Coordination. The first bis-σ adduct **1** was obtained through reaction of the borane H_2BMes with the bis(dihydrogen) complex $Ru(H)_2(H_2)_2(PCy_3)_2$ (Scheme 1). Even though an alternative experimental procedure has been developed, this reaction is important, as it sets the scene for a better understanding of the bonding pattern associated with the formation of the bis-σ adducts. Conceptually, the transformation is the substitution of two coordinated σ(H−H) bonds by two coordinated σ(B−H) ones. In the framework of the Dewar−Chatt−Duncanson model, the interaction of these σ-bonds with the metal center is the result of the synergetic σ-donation from the ligand to the metal and of the π-back-donation from the metal into the σ* orbital (H−H or B−H). Structurally, this results in an elongation of the coordinated σ-bonds. Table 4 shows a comparison between the B−H bond length in the free borane H_2BR (R = Mes, ^{t}Bu, Me, Ph, C_4H_3S) and in the corresponding bis-σ adducts **1**−**5**. There is a clear elongation of the B−H bonds upon coordination by ca. 0.12 Å. Table 4 also reports the reaction energy ΔE_{smd} associated with the substitution of two H_2 molecules by H_2BR (Scheme 1). For all the borane considered, the transformation is exothermic and the reactivity increases in the following order: H_2BMes < H_2B^tBu < $H_2BC_4H_3S$ < H_2BPh < H_2BMe. In order to better understand the origin of this trend, the coordination process has been modeled as a sequence of steps as indicated in Scheme 5.

Scheme 5. Thermodynamic Cycle Associated with the Coordination Process of Ligand L (L = bis-H_2, H_2BR) to the Ru Fragment $[Ru(H)_2(PCy_3)_2]$

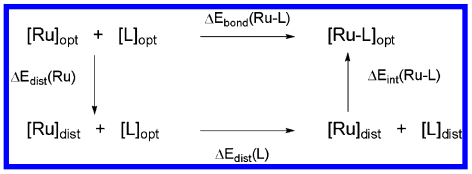

Even though the substitution of the two H_2 ligands by H_2BR is likely to occur stepwise, simultaneous coordination of the two B−H bonds, or the two H_2 ligands, to the $[Ru(H)_2(PCy_3)_2]$ fragment affords easier comparison. In order for the Ru−L bond to be formed (L = $(H_2)_2$, H_2BR), the metal fragment $[Ru(H)_2(PCy_3)_2]$ has to distort from its optimized geometry $[Ru]_{opt}$ to its geometry in the final complex, $[Ru]_{dist}$, and this is associated with a distortion energy ΔE_{dist}(Ru) (see Scheme 5). The same applies for the ligand L, where ΔE_{dist}(L) is the energy needed to bring the optimal geometry of free L, $[L]_{opt}$, to the geometry it adopts once coordinated to Ru, $[L]_{dist}$. The interaction energy ΔE_{int}(Ru−L) corresponds to the energy gained upon formation of the final complex between the two

dx.doi.org/10.1021/om400610k | Organometallics XXXX, XXX, XXX−XXX

distorted fragments $[Ru]_{dist}$ and $[L]_{dist}$. The coordination energy $\Delta E_{bond}(Ru-L)$ is thus obtained as the sum of the contributions from distortions and interaction (eq 1).

$$\Delta E_{bond}(Ru-L) = \Delta E_{dist}(Ru) + \Delta E_{dist}(L) + \Delta E_{int}(Ru-L) \quad (1)$$

The distortion energy of the transition metal fragment $[Ru(H)_2(PCy_3)_2]$ is directly influenced by the size of the ligand L. Coordination of a small ligand like H_2 (and even two H_2) requires less distortion than coordination of bulky ligands like H_2BMes and H_2B^tBu (Table 4). It is interesting to note the impact of the ortho CH_3 groups in H_2BMes with an increase of 6.7 kJ·mol^{-1} of $\Delta E_{dist}(Ru)$ when compared to H_2BPh. The impact of H_2BMe, H_2BPh, and $H_2BC_4H_3S$ on $\Delta E_{dist}(Ru)$ is identical, as these three ligands exert the same steric pressure. The distortion of $Ru(H)_2(PCy_3)_2$ is essentially associated with a change in the P−Ru−P angle. In the optimal geometry of $Ru(H)_2(PCy_3)_2$, the P−Ru−P angle is 173.1°. Coordination of two H_2 molecules induces a bending of the phosphine ligands away from the two H_2 ligands, and the P−Ru−P angle is reduced to 163.6°. The bending is more pronounced for H_2BMe, H_2BPh, and $H_2BC_4H_3S$ with a P−Ru−P angle of 153.8°, thus corresponding to larger $\Delta E_{dist}(Ru)$ values (Table 4). Finally, the larger distortion energies $\Delta E_{dist}(Ru)$ for H_2BMes and H_2B^tBu correspond to even smaller P−Ru−P angles (152.1° and 149.5°, respectively).

A natural bonding orbital (NBO) analysis of the electronic structure of $[Ru]_{opt}$ has been carried out, and Figure 5 shows

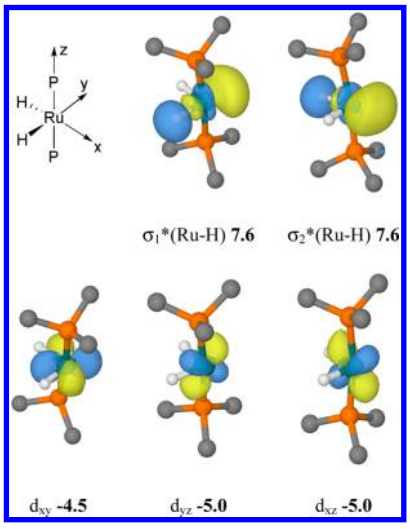

Figure 5. Shape and energy (eV) of the frontier NLMO of the $Ru(H)_2(PCy_3)_2$ fragment.

the shape and energy of selected natural localized molecular orbitals (NLMOs). The metal-centered frontier NLMOs for the d^6 fragment $Ru(H)_2(PCy_3)_2$ are composed of three d lone pairs and two vacant orbitals $\sigma_i^*(Ru-H)$ (i = 1, 2) essentially developed trans to the hydride ligands. The set of pseudo nonbonding occupied NLMOs on Ru is split in two because back-donation into $\sigma^*(P-C)$ orbitals lowers the energy of the d orbital perpendicular to the RuH_2 plane (d_{xz} and d_{yz}).

The coordination of H_2BR to $Ru(H)_2(PCy_3)_2$ proceeds through σ-donation from $\sigma(B-H)$ into $\sigma_i^*(Ru-H)$ and π-back-donation from the equatorial d_{xy} lone pair into $\sigma^*(B-H)$. The essential difference with the bis(dihydrogen) complex is that only one d lone pair (d_{xy}) is used for back-donation into

Table 5. Expression of Selected NLMOs as a Linear Combination of the NBOs[a]

	σ-donation	π-back-donation
$[Ru](H_2)_2$[b]	$\underline{\sigma(H-H)}$ = 0.920 $\sigma(H-H)$ + 0.356 $\sigma^*(Ru-H)$	$\underline{d_{xy}}$ = 0.961 d_{xy} + 0.21 $\sigma^*(H-H)$ $\underline{d_{yz}}$ = 0.972 d_{yz} + 0.201 $\sigma^*(H-H)$
1	$\underline{\sigma(B-H)}$ = 0.930 $\sigma(B-H)$ + 0.33 $\sigma^*(Ru-H)$	$\underline{d_{xy}}$ = 0.978 d_{xy} + 0.12($\sigma_1^*(B-H)$ + $\sigma_2^*(B-H)$) $\underline{d_2}$ = 0.907 d_{yz} + 0.376 LP*(B)
2	$\underline{\sigma(B-H)}$ = 0.928 $\sigma(B-H)$ + 0.334 $\sigma^*(Ru-H)$	$\underline{d_{xy}}$ = 0.976 d_{xy} + 0.129($\sigma_1^*(B-H)$ + $\sigma_2^*(B-H)$) $\underline{d_2}$ = 0.894 d_{yz} + 0.366 LP*(B)
3	$\underline{\sigma(B-H)}$ = 0.927 $\sigma(B-H)$ + 0.336 $\sigma^*(Ru-H)$	$\underline{d_{xy}}$ = 0.978 d_{xy} + 0.118($\sigma_1^*(B-H)$ + $\sigma_2^*(B-H)$) $\underline{d_2}$ = 0.870 d_{yz} + 0.390 LP*(B)
4	$\underline{\sigma(B-H)}$ = 0.929 $\sigma(B-H)$ + 0.329 $\sigma^*(Ru-H)$	$\underline{d_{xy}}$ = 0.975 d_{xy} + 0.132($\sigma_1^*(B-H)$ + $\sigma_2^*(B-H)$) $\underline{d_2}$ = 0.906 d_{yz} + 0.378 LP*(B)
5	$\underline{\sigma(B-H)}$ = 0.933 $\sigma(B-H)$ + 0.320 $\sigma^*(Ru-H)$	$\underline{d_{xy}}$ = 0.977 d_{xy} + 0.124($\sigma_1^*(B-H)$ + $\sigma_2^*(B-H)$) $\underline{d_2}$ = 0.904 d_{yz} + 0.379 LP*(B)

[a]For σ-donation from $\sigma(X-H)$ (X = H, B) into $\sigma^*(Ru-H)$, two slightly different expressions were obtained, but the average of the coefficients is given below. See text for definition of d_2 and LP*(B). [b]$[Ru](H_2)_2 = RuH_2(H_2)_2(PCy_3)_2$.

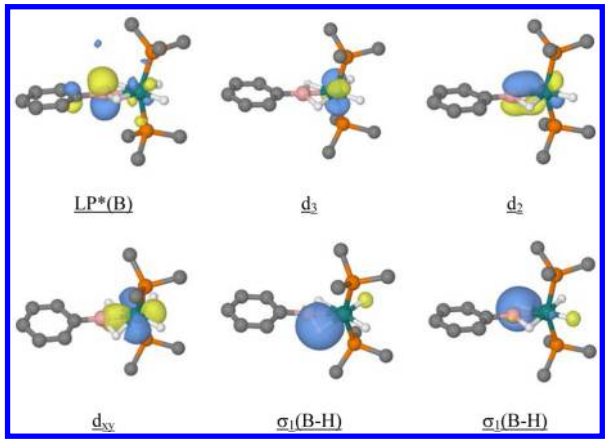

Figure 6. Shape of selected NLMOs of **3**.

$\sigma^*(B-H)$ because of the geometry imposed by H_2BR. Table 5 gives the composition of the NLMOs associated with σ-donation from $\sigma(X-H)$ (with X = H, B) and back-donation into $\sigma^*(X-H)$ for the various complexes, and Figure 6 displays the corresponding NLMOs in the case of H_2BPh. From the values in Table 5, one can conclude that σ-donation from H_2 is slightly larger than from any borane as the weight of the parent NBO is lower. In the same spirit, back-donation from d_{xy} and d_{yz} in the bis(dihydrogen) complex is stronger than back-donation from d_{xy} in the borane complexes. Yet, the interaction energy values $\Delta E_{int}(Ru-L)$ are more negative for **1**−**5**, and the substitution of H_2 by borane is exothermic. This extra gain of stability originates from the π-acid properties at boron with a pseudovacant orbital centered on boron and perpendicular to the BH_2 plane, LP*(B). The two isoenergetic d orbitals d_{yz} and d_{xz}, can mix to transform into two equivalent d orbitals, d_2 and d_3, with d_2 having the correct symmetry to interact with the vacant orbital at boron and d_3 remaining essentially non-bonding (Figure 6). The interaction between d_2 and LP*(B) is significant, as illustrated by the expression of the resulting

dx.doi.org/10.1021/om400610k | Organometallics XXXX, XXX, XXX−XXX

NLMO d_2 (Table 5, Figure 6). This strong interaction is responsible for the short Ru−B distance observed experimentally. Back-donation into σ^*(B−H) is efficient from d_{xy}, as the borane ligand lies in the equatorial plane. From the expression of the NLMOs and from the values of ΔE_{int}(Ru−L) (Table 4), there are two distinct groups: aromatic and aliphatic boranes. The former experiences weaker back-donation from the metal center because the vacancy at boron is destabilized by conjugation with the aromatic ring. Such an interaction is clearly visible in the shape of the NLMO (LP*(B) in Figure 6). For the aliphatic cases, the only source of stabilization of the vacancy at boron in free H_2BR is through hyperconjugation. This is effective in H_2B^tBu and H_2BMe, where one C−X bond (X = H, for Me; X = C, for ^{t}Bu) is aligned with the p OA on boron. This C−X bond is elongated with respect to the two other ones (1.106 Å vs 1.094 Å, Me; 1.559 Å vs 1.534 Å, ^{t}Bu) and presents a reduced B−C−X angle (104.0° vs 115° Me; 98.4° vs 114.5°, ^{t}Bu). This hyperconjugation is not strong enough to compete with back-donation from d_2, and the NBO analysis even found a bond, constructed on d_2 and LP*(B), between Ru and B. This illustrates the greater π-acidity of the aliphatic boranes.

CONCLUSION

In summary, we have shown that the geminal bis(σ-B−H) coordination mode between a monosubstituted borane (RBH_2) and a [$RuH_2(PR'_3)_2$] ruthenium fragment could be obtained with different phosphines and a variety of boron substituents. The corresponding complexes $RuH_2(\eta^2{:}\eta^2\text{-}H_2BR)(PR'_3)_2$ were conveniently synthesized in a one-pot procedure by the use of lithium monosubstituted borohydrides RBH_3Li and the chloro complexes $RuHCl(H_2)(PR'_3)_2$, thus enabling an easy access to this class of compounds. Although the obtained complexes present similar spectroscopic and structural data, complex **2** exhibits original behavior in solution; it is involved in an equilibrium with the κ^3*H-tert*-butylborohydride form **2′** that is very close in energy. In contrast, the presence at boron of a thienyl group with a sulfur atom likely to coordinate to the metal center does not favor an agostic species such as **5″** and neither a borohydride linkage as in **2′** or as previously reported.[29] In our systems, borane coordination to the metal center proceeds predominantly through σ-donation from σ(B−H) into σ_i^*(Ru−H) and π-back-donation from the equatorial d_{xy} lone pair into σ^*(B−H), the borane ligand being forced to lie in the equatorial plane for better orbital overlap. NBO analysis well evidenced the greater π-acidity of the aliphatic boranes. The geminal bis(σ-B−H) coordination mode represents a first level in the B−H bond activation of monosubstituted boranes, and future work will address reactivity studies toward more pronounced degrees of B−H activation.

EXPERIMENTAL SECTION

General Procedures. All experiments were performed under an atmosphere of dry argon using standard Schlenk and glovebox techniques. Unless stated, all chemicals were purchased from Aldrich and used without further purification. [$RuH_2(\eta^2\text{-}H_2)_2(PCy_3)_2$],[38] [$RuHCl(\eta^2\text{-}H_2)(PCy_3)_2$],[26] [$RuHCl(\eta^2\text{-}H_2)(P^iPr_3)_2$],[26] and lithium borohydrides (RBH_3Li)[27] were prepared according to literature procedures. THF was freshly distilled under argon from Na/benzophenone. All other solvents were purified and dried through an activated alumina purification system (MBraun SPS-800). NMR solvents were dried using appropriate methods and degassed prior to use. NMR samples of sensitive compounds were prepared under an argon atmosphere. Nuclear magnetic resonance spectra were recorded on Bruker AV 300, 400, or 500 spectrometers operating at 300.13, 400.13, or 500.33 MHz, respectively, for ^{1}H; 121.5, 161.97, or 202.5 MHz, respectively, for ^{31}P; 75.48, 100.62, or 125.81 MHz, respectively, for ^{13}C; and 96.29, 128.38, or 160.52 MHz, respectively, for ^{11}B. ^{1}H and ^{13}C chemical shifts are reported in ppm referenced internally to residual protiosolvent, while ^{31}P chemical shifts are relative to 85% H_3PO_4 and those of ^{11}B are relative to $BF_3{\cdot}OEt_2$ external references. Chemical shifts are quoted in δ (ppm), and coupling constants in hertz. The following abbreviations are used: br, broad; s, singlet; d, doublet; t, triplet; m, multiplet. Infrared spectra were recorded on a Bruker Alpha FT-IR spectrometer equipped with a Platinum single reflection ATR module. Elemental analyses were performed by the "in-house" service of the Laboratoire de Chimie de Coordination, Toulouse

$RuHCl(\eta^2\text{-}H_2)(PCyp_3)_2$. A mixture of $[Ru(COD)Cl_2]_n$ (1.00 g, 3.6 mmol), tricyclopentylphosphine (1.73 mL, 7.2 mmol), triethylamine (0.50 mL, 3.6 mmol), and 2-propanol (20 mL) was heated at 85 °C overnight in a Fischer−Porter bottle pressurized under dihydrogen (2.5 bar). After cooling at −40 °C, the suspension was filtered. The brown solid was washed with cold ether and dried under vacuum (1.84 g, 84%).

$^{31}P\{^1H\}$ NMR (C_6D_6, 298 K, 162 MHz): δ 54.84 (s, $PCyp_3$). ^{1}H NMR (C_6D_6, 298 K, 400 MHz): −16.43 (s, 3H, $RuH(H_2)$), 1.5−2.4 (m, 54H, Cyp). $^{13}C\{^1H\}$ NMR (C_6D_6, 298 K, 100 MHz): 26.45 (vt, $^{app}J_{PC}$ = 4.0 Hz, CH_2 Cyp), 30.33 (vt, $^{app}J_{PC}$ < 2 Hz, CH_2 Cyp), 36.71 (vt, $^{app}J_{PC}$ = 11 Hz, PCH Cyp).

$RuH_2(\eta^2{:}\eta^2\text{-}H_2BMe)(PCy_3)_2$ (3). An ethereal solution (2 mL) of $MeBH_3Li$ (35.1 mg, 0.419 mmol) was added to a suspension of $RuHCl(\eta^2\text{-}H_2)(PCy_3)_2$ (293.4 mg, 0.419 mmol) in ether (4 mL) and stirred at room temperature for 5 min. After removal of the solvent under vacuum, pentane was added, affording a suspension that was filtered over activated Celite. The solvent was then removed under vacuum, leading to $RuH_2(\eta^2{:}\eta^2\text{-}BH_2Me)(PCy_3)_2$ (**3**) (259.3 mg, 90%) as an orange-brown powder. ^{1}H NMR (C_6D_6, 400,13 MHz): −11.06 (t, 2H, $^2J_{PH}$ = 25.6 Hz, RuH_2), −6.22 (br, 2H, RuH_2B), 0.82 (s, 3H, Me), 1.20−2.50 (m, 66H, Cy). $T_{1\ min}$ (tol-d_8, 253 K, 500.33 MHz): −11.06 (344 ms), −6.22 (173 ms). $^{13}C\{^1H\}$ NMR (C_6D_6, 100.62 MHz): 11.66 (CH_3), 27.01, 28.05, 30.70 (CH_2, PCy_3), 38.81 (CH, PCy_3). $^{31}P\{^1H\}$ NMR (C_6D_6, 161.99 MHz): 81.48 (s). $^{11}B\{^1H\}$ NMR (C_6D_6, 128.38 MHz): 66.4 (br). Anal. Calcd for $C_{37}H_{73}BP_2Ru$: C, 64.24; H, 10.64. Found: C, 63.62; H, 11.46.

$RuH_2(\eta^2{:}\eta^2\text{-}H_2BPh)(PCy_3)_2$ (4). Toluene (5 mL) was added to a mixture of $RuHCl(\eta^2\text{-}H_2)(PCyp_3)_2$ (72.2 mg, 0,103 mmol) and lithium phenylborohydride, $PhBH_3Li$ (12.0 mg, 0.122 mmol). The solution was stirred at room temperature for 17 h and filtrated over Celite. A minimum amount of pentane was added, and the suspension was stirred. After removal of the pentane supernatant, the yellow solid was dried under vacuum. Compound **4** was isolated as a yellow powder in 71% yield (55 mg). ^{1}H NMR (C_6D_6, 298 K, 400 MHz): −11.11 (td, 2H, $^2J_{PH}$ = 25.2 Hz, J_{HH} = 3.5 Hz RuH_2), −5.6 (brs, 2H, RuH_2B), 1.3−2.3 (m, 66H, Cy), 7.28−7.36 (m, 3H, CH Ph), 8.17 (m, 2H, CH Ph). $^{13}C\{^1H\}$ NMR (C_6D_6, 298 K, 100.62 MHz): 27.0, 27.95, 30.71 (CH_2 Cy), 38.80 (m, CH Cy), 127.92, 129.87, 135.82 (s, CH Ph), the *ipso*-$C^{IV}B$ was not observed. $^{31}P\{^1H\}$ NMR (C_6D_6, 298 K, 161.97 MHz): 81.60 (s, PCy_3). $^{11}B\{^1H\}$ NMR (C_6D_6, 298 K, 128.38 MHz): 61.4 (brs). Anal. Calcd for $C_{42}H_{75}BP_2Ru$: C, 66.91; H, 10.03. Found: C, 67.75; H, 10.00.

$RuH_2(\eta^2{:}\eta^2\text{-}H_2BC_4H_3S)(PCy_3)_2$ (5). Ether (5 mL) was added to a mixture of 2-thienylborohydride (2-$C_4H_3SBH_3Li$) (34 mg, 0.286 mmol) and $RuHCl(\eta^2\text{-}H_2)(PCy_3)_2$ (200.0 mg, 0.286 mmol), and the resulting yellow solution was stirred for 1 h at room temperature. After removal of the solvent under vacuum and addition of toluene (8 mL), the resulting suspension was filtered over Celite. The solvent was removed under vacuum, affording a yellow solid. This solid was washed with a minimum amount of pentane and dried under vacuum to afford pure $RuH_2(\eta^2{:}\eta^2\text{-}H_2BC_4H_3S)(PCy_3)_2$, which was isolated as an orange-yellow solid (175 mg, 81%).

^{1}H NMR (THF-d_8, 400.13 MHz): −11.95 (td, 2H, $^2J_{PH}$ = 25.2 Hz, J_{HH} = 2.4 Hz, RuH_2), −5.80 (br, 2H, RuH_2B), 1.20−2.10 (m, 66H, Cy), 7.10 (dd, 1H, $^3J_{HH}$ = 2.4 Hz, $^3J_{HH}$ = 4.5 Hz, CH^4 thienyl), 7.51 (d, 1H, $^3J_{HH}$ = 2.4 Hz, CH^3 thienyl), 7.63 (d, 1H, $^3J_{HH}$ = 4.5 Hz, CH^5

dx.doi.org/10.1021/om400610k | *Organometallics* XXXX, XXX, XXX−XXX

thienyl). $T_{1\,min}$ (tol-d_8, 253 K, 500.33 MHz): −11.55 (357 ms), −5.46 (157 ms). $^{13}C\{^1H\}$ NMR (THF-d_8, 100.62 MHz): 26.73, 27.70, 30.37 (CH_2 PCy_3), 38.48 (m, CH PCy_3), 127.78 (s, C^4H thienyl), 131.31 (s, C^5H thienyl), 136.60 (s, C^3H thienyl), 148.37 (br, *ispo*-C^2B thienyl). $^{31}P\{^1H\}$ NMR (THF-d_8, 161.97 MHz): 80.27 (s). $^{11}B\{^1H\}$ NMR (THF-d_8, 128.38 MHz): 54 (br). Anal. Calcd for $C_{40}H_{73}BP_2RuS$: C, 63.22; H, 9.68. Found: C, 63.20; H, 9.39.

$RuH_2(\eta^2{:}\eta^2\text{-}H_2BMes)(P^iPr_3)_2$ (6). Ether (15 mL) was added to a mixture of $RuHCl(\eta^2\text{-}H_2)(P^iPr_3)_2$ (300 mg, 0.652 mmol) and lithium mesitylborohydride, $MesBH_3Li$ (91.3 mg, 0.652 mmol), and the solution was stirred at room temperature for 15 min. The resulting suspension was filtrated over Celite, and the solvent removed under vacuum, affording a yellow solid. Pentane was added at −25 °C. Addition of cold pentane (−25 °C) afforded a precipitate that was separated from the supernatant. After drying under vacuum, **6** was isolated as a yellow solid (210 mg, 58% yield). ^1H NMR (C_6D_6, 298 K, 300 MHz): −11.24 (td, 2H, $^2J_{PH}$ = 25.4 Hz, J_{HH} = 3.0 Hz, RuH_2), −6.04 (brs, 2H, RuH_2B), 1.19 (m, 36, $^3J_{HH}$ = 6.8 Hz, CH_3 ^{i}Pr), 2.01 (m, 6H, $^3J_{HH}$ = 6.8 Hz, CH ^{i}Pr), 2.17 (s, 3H, *p*-CH_3 Mes), 2.96 (s, 6H, *o*-CH_3 Mes), 6.87 (s, 2H, CH Mes). $^{13}C\{^1H\}$ NMR (C_6D_6, 298 K, 100.62 MHz): 20.40 (s, CH_3 ^{i}Pr), 21.10 (s, *p*-CH_3 Mes), 23.06 (s, *o*-CH_3 Mes), 28.31 (m, Hz, CH ^{i}Pr), 128.89 (s, CH Mes), 139.66 (s, p-C^{IV} Mes), 144.76 (s, o-C^{IV} Mes), the *ipso*-$C^{IV}B$ was not observed. $^{31}P\{^1H\}$ NMR (C_6D_6, 298 K, 121.5 MHz): 96.84 (s). $^{11}B\{^1H\}$ NMR (C_6D_6, 298 K, 128.38 MHz): 57 (brs). Anal. Calcd for $C_{27}H_{57}BP_2Ru$: C, 58.37; H, 10.34. Found: C, 58.57; H, 10.71.

$RuH_2(\eta^2{:}\eta^2\text{-}H_2BMes)(PCyp_3)_2$ (7). Ether (15 mL) was added to a mixture of $RuHCl(\eta^2\text{-}H_2)(PCyp_3)_2$ (400 mg, 0,649 mmol) and lithium mesitylborohydride, $MesBH_3Li$ (113.6 mg, 0.649 mmol). The resulting solution was stirred at room temperature for 15 min. Then, the solvent was evaporated under vacuum, and toluene (10 mL) was added. The resulting suspension was filtered over Celite, and the solvent removed under vacuum. Pentane was added and removed again under vacuum. After drying, **7** was isolated as a yellow solid (58% yield, 268 mg). ^1H NMR (C_6D_6, 298 K, 400 MHz): −11.08 (t, 2H, $^2J_{PH}$ = 25.4 Hz, RuH_2), −6.18 (brs, 2H, RuH_2B), 1.5−2.1 (m, Cyp), 2.15 (s, 3H, *p*-CH_3 Mes), 2.97 (s, 6H, *o*-CH_3 Mes), 6.87 (s, 2H, *m*-H Mes). $^{13}C\{^1H\}$ NMR (C_6D_6, 298 K, 100.62 MHz): 21.22 (s, *p*-CH_3 Mes), 23.20 (s, *o*-CH_3 Mes), 26.34, 30.46 (CH_2 Cyp), 41.14 (CH Cyp), 129.04 (s, CH Mes), 139.83 (s, *p*-C^{IV} Mes), 144.78 (s, *o*-C^{IV} Mes), the *ipso*-$C^{IV}B$ was not observed. $^{31}P\{^1H\}$ NMR (C_6D_6, 298 K, 161.97 MHz): 88.77 (s). $^{11}B\{^1H\}$ (C_6D_6, 298 K, 128.38 MHz): 57.5 (brs). Anal. Calcd for $C_{39}H_{69}BP_2Ru$: C, 65.81; H, 9.77. Found: C, 65.01; H, 10.23.

Computational Details. All the calculations have been performed with the Gaussian09 package at the B3PW91 level of hybrid density functional theory.[39−41] For the optimization of geometry, the ruthenium atom was represented by the relativistic effective core potential (RECP) from the Stuttgart group and the associated basis sets,[42] augmented by an f polarization function.[43] The phosphorus and sulfur atoms were represented by the RECP from the Stuttgart group and the associated basis set,[44] augmented by a d polarization function.[45] The remaining atoms (C, H, B) were represented by a 6-31G(d,p) basis set. The solvent (toluene) influence was taken into consideration through single-point calculations on the gas-phase-optimized geometry with IEFPCM calculations.[46] For the IEFPCM calculations the basis set on Ru was kept as in the gas-phase optimizations, but the remaining atoms were treated with a 6-311+G(d,p) basis set. The SMD model by Truhlar et al. was used in the IEFPCM calculations.[47] The NBO analysis was performed with the NBO6 version.[48]

■ ASSOCIATED CONTENT

Supporting Information

NMR data; computational details, Cartesian coordinates, and energy of the optimized structures; and X-ray data. The five crystal structures have been deposited at the Cambridge Crystallographic Data Centre and allocated the deposition numbers CCDC 946541−946545. This material is available free of charge via the Internet at http://pubs.acs.org.

■ AUTHOR INFORMATION

Corresponding Author

*E-mail: gilles.alcaraz@lcc-toulouse.fr, eric.clot@univ-montp2.fr, sylviane.sabo@lcc-toulouse.fr.

Present Address

⊥Leibniz-Institut für Oberflächenmodifizierung e.V. Permoserstrasse 15, D-04318 Leipzig, Germany.

Notes

The authors declare no competing financial interest.

■ ACKNOWLEDGMENTS

We thank the CNRS (G.A. and S.S.E.), the ANR (programme HyBoCat, ANR-09-BLAN-0184), and the French Ministry of Research (Y.G.) for support, and the DGA for the salary of G.B.-L. Johnson Matthey is gratefully acknowledged for a generous gift of $RuCl_3{\cdot}nH_2O$.

■ REFERENCES

(1) Alcaraz, G.; Clot, E.; Helmstedt, U.; Vendier, L.; Sabo-Etienne, S. *J. Am. Chem. Soc.* **2007**, *129*, 8704−8705.

(2) Alcaraz, G.; Grellier, M.; Sabo-Etienne, S. *Acc. Chem. Res.* **2009**, *42*, 1640−1649.

(3) Alcaraz, G.; Vendier, L.; Clot, E.; Sabo-Etienne, S. *Angew. Chem., Int. Ed.* **2010**, *49*, 918−920.

(4) Alcaraz, G.; Chaplin, A. B.; Stevens, C. J.; Clot, E.; Vendier, L.; Weller, A. S.; Sabo-Etienne, S. *Organometallics* **2010**, *29*, 5591−5595.

(5) Alcaraz, G.; Sabo-Etienne, S. *Angew. Chem., Int. Ed.* **2010**, *49*, 7170−7179.

(6) MacInnis, M. C.; McDonald, R.; Ferguson, M. J.; Tobisch, S.; Turculet, L. *J. Am. Chem. Soc.* **2011**, *133*, 13622−13633.

(7) Sewell, L. J.; Lloyd-Jones, G. C.; Weller, A. S. *J. Am. Chem. Soc.* **2012**, *134*, 3598−3610.

(8) Stevens, C. J.; Dallanegra, R.; Chaplin, A. B.; Weller, A. S.; Macgregor, S. A.; Ward, B.; McKay, D.; Alcaraz, G.; Sabo-Etienne, S. *Chem.—Eur. J.* **2011**, *17*, 3011−3020.

(9) Tang, C. Y.; Thompson, A. L.; Aldridge, S. *Angew. Chem., Int. Ed.* **2010**, *49*, 921−925.

(10) Tang, C. Y.; Thompson, A. L.; Aldridge, S. *J. Am. Chem. Soc.* **2010**, *132*, 10578−10591.

(11) Staubitz, A.; Robertson, A. P. M.; Manners, I. *Chem. Rev.* **2010**, *110*, 4079−4124.

(12) Stephens, F. H.; Pons, V.; Baker, R. T. *Dalton Trans.* **2007**, 2613−2626.

(13) Kubas, G. J. *Metal Dihydrogen and sigma-Bond Complexes*; Kluwer Academic/Plenum Publishers: New York, 2001; p 444.

(14) Hartwig, J. F.; Muhoro, C. N.; He, X.; Eisenstein, O.; Bosque, R.; Maseras, F. *J. Am. Chem. Soc.* **1996**, *118*, 10936−10937.

(15) Montiel-Palma, V.; Lumbierres, M.; Donnadieu, B.; Sabo-Etienne, S.; Chaudret, B. *J. Am. Chem. Soc.* **2002**, *124*, 5624−5625.

(16) Lachaize, S.; Essalah, K.; Montiel-Palma, V.; Vendier, L.; Chaudret, B.; Barthelat, J. C.; Sabo-Etienne, S. *Organometallics* **2005**, *24*, 2935−2943.

(17) Essalah, K.; Barthelat, J.-C.; Montiel, V.; Lachaize, S.; Donnadieu, B.; Chaudret, B.; Sabo-Etienne, S. *J. Organomet. Chem.* **2003**, *680*, 182−187.

(18) Hebden, T. J.; Denney, M. C.; Pons, V.; Piccoli, P. M. B.; Koetzle, T. F.; Schultz, A. J.; Kaminsky, W.; Goldberg, K. I.; Heinekey, D. M. *J. Am. Chem. Soc.* **2008**, *130*, 10812−10820.

(19) Hesp, K. D.; Rankin, M. A.; McDonald, R.; Stradiotto, M. *Inorg. Chem.* **2008**, *47*, 7471−7473.

(20) Gloaguen, Y.; Alcaraz, G.; Vendier, L.; Sabo-Etienne, S. *J. Organomet. Chem.* **2009**, *694*, 2839−2841.

(21) Abdur-Rashid, K.; Gusev, D. G.; Lough, A. J.; Morris, R. H. *Organometallics* **2000**, *19*, 1652−1660.

(22) Grellier, M.; Vendier, L.; Chaudret, B.; Albinati, A.; Rizzato, S.; Mason, S.; Sabo-Etienne, S. *J. Am. Chem. Soc.* **2005**, *127*, 17592−17593.
(23) Oliván, M.; Clot, E.; Eisenstein, O.; Caulton, K. G. *Organometallics* **1998**, *17*, 3091−3100.
(24) Pasto, D. J.; Lepeska, B.; Balasubramaniyan, V. *J. Am. Chem. Soc.* **1972**, *94*, 6090−6096.
(25) Srebnik, M.; Cole, T. E.; Ramachandran, P. V.; Brown, H. C. *J. Org. Chem.* **1989**, *54*, 6085−6096.
(26) Wolf, J.; Stüer, W.; Grünwald, C.; Gevert, O.; Laubender, M.; Werner, H. *Eur. J. Inorg. Chem.* **1998**, *1998*, 1827−1834.
(27) Singaram, B.; Cole, T. E.; Brown, H. C. *Organometallics* **1984**, *3*, 774−777.
(28) Alcaraz, G.; Sabo-Etienne, S. *Coord. Chem. Rev.* **2008**, *252*, 2395−2409.
(29) Gloaguen, Y.; Alcaraz, G.; Pécharman, A.-F.; Clot, E.; Vendier, L.; Sabo-Etienne, S. *Angew. Chem., Int. Ed.* **2009**, *48*, 2964−2968.
(30) Gloaguen, Y.; Alcaraz, G.; Petit, A. S.; Clot, E.; Coppel, Y.; Vendier, L.; Sabo-Etienne, S. *J. Am. Chem. Soc.* **2011**, *133*, 17232−17238.
(31) Cole, T. E.; Bakshi, R. K.; Srebnik, M.; Singaram, B.; Brown, H. C. *Organometallics* **1986**, *5*, 2303−2307.
(32) Perrin, L.; Clot, E.; Eisenstein, O.; Loch, J.; Crabtree, R. H. *Inorg. Chem.* **2001**, *40*, 5806−5811.
(33) Zaidlewicz, M.; Brown, H. C. *Organic Syntheses via Boranes*; Aldrich Chemical Co., Inc.: Milwaukee, WI, 2001; Vol. *2*, p 374.
(34) Marks, T. J.; Kolb, J. R. *Chem. Rev.* **1977**, *77*, 263−293.
(35) Besora, M.; Lledós, A. Contemporary Metal Boron Chemistry I. Borylenes, Boryls, Borane σ-Complexes, and Borohydrides, Structure and Bonding. In *Structure and Bonding (Berlin)*; Mingos, D. M. P., Ed.; Springer: Berlin, 2008; Vol. *130*, pp 149−202.
(36) Hesp, K. D.; Kannemann, F. O.; Rankin, M. A.; McDonald, R.; Ferguson, M. J.; Stradiotto, M. *Inorg. Chem.* **2011**, *50*, 2431−2444.
(37) Borowski, A. F.; Donnadieu, B.; Daran, J.-C.; Sabo-Etienne, S.; Chaudret, B. *Chem. Commun.* **2000**, 543−544.
(38) Borowski, A. F.; Sabo-Etienne, S.; Christ, M. L.; Donnadieu, B.; Chaudret, B. *Organometallics* **1996**, *15*, 1427−1434.
(39) Frisch, M. J.; Trucks, G. W.; Schlegel, H. B.; Scuseria, G. E.; Robb, M. A.; Cheeseman, J. R.; Scalmani, G.; Barone, V.; Mennucci, B.; Petersson, G. A.; et al. *Gaussian 09*, Revision B1; Gaussian Inc.: Wallingford, CT, 2009.
(40) Becke, A. D. *J. Chem. Phys.* **1993**, *98*, 5648−5652.
(41) Perdew, J. P.; Wang, Y. *Phys. Rev. B: Condens. Matter* **1992**, *45*, 13244−13249.
(42) Andrae, D.; Häußermann, U.; Dolg, M.; Stoll, H.; Preuß, H. *Theor. Chim. Acta* **1990**, *77*, 123−141.
(43) Ehlers, A. W.; Böhme, M.; Dapprich, S.; Gobbi, A.; Höllwarth, A.; Jonas, V.; Köhler, K. F.; Stegmann, R.; Veldkamp, A.; Frenking, G. *Chem. Phys. Lett.* **1993**, *208*, 111−114.
(44) Bergner, A.; Dolg, M.; Küchle, W.; Stoll, H.; Preuß, H. *Mol. Phys.* **1993**, *80*, 1431−1441.
(45) Höllwarth, A.; Böhme, M.; Dapprich, S.; Ehlers, A. W.; Gobbi, A.; Jonas, V.; Köhler, K. F.; Stegmann, R.; Veldkamp, A.; Frenking, G. *Chem. Phys. Lett.* **1993**, *208*, 237−240.
(46) Tomasi, J.; Mennucci, B.; Cammi, R. *Chem. Rev.* **2005**, *105*, 2999−3094.
(47) Marenich, A. V.; Cramer, C. J.; Truhlar, D. G. *J. Phys. Chem. B* **2009**, *113*, 6378−6396.
(48) Glendening, E. D.; Badenhoop, J. K.; Reed, A. E.; Carpenter, J. E.; Bohmann, J. A.; Morales, C. M.; Landis, C. R.; Weinhold, F. *NBO 6.0*; Theoretical Chemistry Institute, University of Wisconsin: Madison, WI; http://nbo6.chem.wisc.edu/, 2013.